Soft Matter

Elasto-morphology of P3HT:PCBM Bulk Heterojunction Organic Solar Cells

Journal:	*Soft Matter*
Manuscript ID	SM-ART-05-2020-000849.R1
Article Type:	Paper
Date Submitted by the Author:	10-Jun-2020
Complete List of Authors:	Munshi, Joydeep; Lehigh University, Mechanical Engineering Chien, TeYu; University of Wyoming, Physics and Astronomy Chen, Wei; Northwestern University Balasubramanian, Ganesh; Lehigh University, Mechanical Engineering; Lehigh University,

Elasto-morphology of P3HT:PCBM Bulk Heterojunction Organic Solar Cells

Joydeep Munshi[1], TeYu Chien[2], Wei Chen[3] and Ganesh Balasubramanian[1, Γ]

[1]*Department of Mechanical Engineering & Mechanics, Lehigh University, Bethlehem, PA, USA 18015*

[2]*Department of Physics & Astronomy, University of Wyoming, Laramie, WY, USA 82071*

[3]*Department of Mechanical Engineering, Northwestern University, Evanston, IL, USA 60208*

Abstract

Predicting the mechanical properties of organic semiconductors is important to employ these materials in flexible electronics applications. For instance, knowledge of the mechanical and thermal stability of thin film organic solar cells (OSCs) is critical for roll-to-roll production of photovoltaic devices and its use under various operating conditions. We examine the thermal and elasto-mechanical properties of conjugated donor polymer poly-(3-hexylthiophene) (P3HT) and interpenetrating mixtures of P3HT and phenyl-C61-butyric acid methyl ester (PCBM) bulk heterojunction (BHJ) active layers under an applied unidirectional tensile deformation using coarse-grained molecular dynamics (CGMD) simulations. The predictions are validated against previous experimental reports as well as with earlier modeling results derived using different intermolecular forcefields. Our results reveal that PCBM molecules behave as anti-plasticizers when mixed with P3HT and tend to increase the tensile modulus and glass transition temperature, while decreasing the crack-onset strain relative to pure P3HT. The variations in the mechanical properties with composition of the BHJ active layer suggest that in presence of small oligomers as

Γ Corresponding author. Email: bganesh@lehigh.edu. Phone: +1-610-758-3784.

Address: Packard Laboratory 561, 19 Memorial Drive West, Bethlehem, PA 18015, USA.

additives in the BHJ, P3HT:PCBM mixture resists the anti-plasticizing effect of PCBM molecules due to low tensile modulus of the short polymer chains.

Keywords: *P3HT:PCBM, morphology, elastic modulus, glass transition, organic solar cell, coarse-grained molecular dynamics*

1. Introduction

Photovoltaic (PV) materials have contributed to considerable advances towards carbon-free clean energy conversion [1, 2]. Amongst them, organic solar cells (OSCs) are attractive due to their low-temperature solution processability, light weight and device flexibility [3-5]. OSCs consisting of an interpenetrating mixture of electron donors (e.g., semiconducting polymers) and electron acceptor (e.g., fullerene) photoactive layers, a.k.a. bulk heterojunction (BHJ), exhibit the most promising morphologies due to their high power conversion efficiency (PCE) [6]. Nevertheless, extensive research over the past decade has increased the PCE of OSCs with BHJ architectures to a paltry ~10 % [7-9], while a recent effort reports that tandem structure composed of double BHJs enhances the PCE up to 15 % [10]. PCE depends on the morphology of BHJ and intermolecular interactions of the active layer constituents [11, 12], and numerous studies have probed the correlations between BHJ structure, property and performance [13-18].

On the other side of the coin, organic semiconductors being mechanically compliant and thermally stable, hold the potential for designing lightweight, portable and flexible OSC devices [19-22]. Despite several experimental [23-28] and computational investigations [29-31] to understand the effect of processing parameters on morphology and performance of OSCs, there still remains a gap in the understanding on how these factors affect the thermo- and elasto-mechanical properties of these energy conversion devices. To bridge the space between experimental measurements and predictions from atomistic simulations, coarse-grained molecular dynamics (CGMD) can be employed to examine the thermomechanical properties of polymeric systems [32]. CGMD simulations are able to simulate larger system sizes for longer times approaching experimental scales. Here, we present results from CGMD simulations of a representative solvent-free mixture of poly-(3-hexyl-thiophene) (P3HT) and phenyl-C_{61}-butyric acid methyl ester (PCBM) that

compose the BHJ morphology. Thermally annealed pure P3HT and P3HT:PCBM BHJ morphology are subjected to unidirectional tensile strains to scrutinize the stress-strain behavior. We find that while simulation results for elastic modulus, density and glass transition temperature (T_g) agree with prior experimental reports, addition of oligomers decreases the tensile modulus and T_g due to the plasticizing effect of the small polymer molecules.

2. Computational Methods

P3HT, PCBM and Chlorobenzene (CB) molecules are modeled using the coarse-grained beads as described by the Martini force field [13, 33] extended to polymers, fullerene and benzene rings [34-36]. The typical force field parameters are from ref [13] and listed in Table S1 in the supporting information. While the effect of CG model resolution can affect the calculated elastic properties, predictions for the tensile modulus and density of P3HT and P3HT:PCBM BHJ from the three-site model [15] are found to concur with experiments [29]. We employ the improved Martini force field that considers finer CG mapping relative to earlier approaches while retaining certain chemical specificity such as the anisotropy of the thiophene backbone ring [13]. The computational procedure adopted to mimic a typical spin-coating process to prepare P3HT:PCBM BHJ structure is described in detailed in our earlier reports[17, 18, 37] and as supplementary information. Nonequilibrium (NE-CGMD) simulations are employed by introducing a constant velocity of deformation (~ 1×10^{-4} nm/ps) along the longitudinal (*x*-) direction to simulate unidirectional tension as illustrated in Figure 1. Our choice of deformation velocity, corresponding to a strain rate ~ 1×10^{-5} ps^{-1}, is necessitated by the lowest achievable strain rate given the time scale in CGMD simulations.

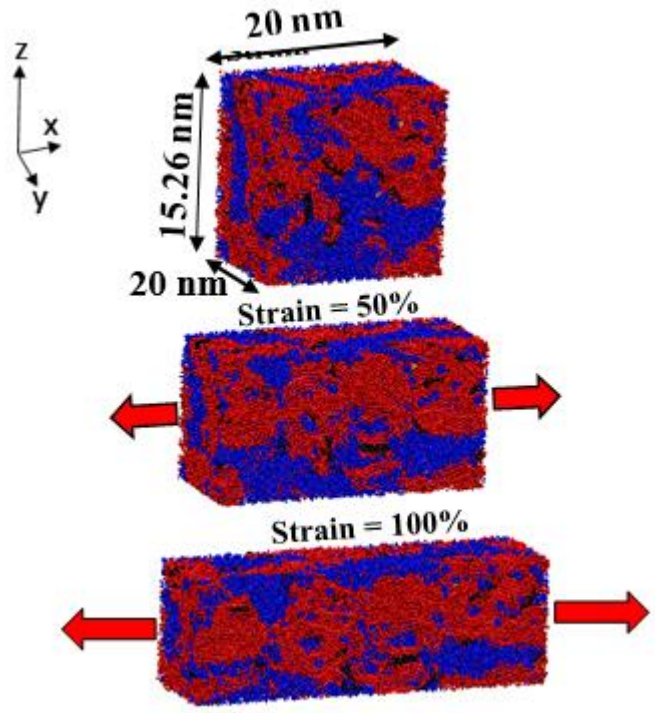

Figure 1: *Simulated unidirectional tension of thermally annealed P3HT:PCBM BHJ morphology (P3HT is represented by red beads and PCBM is represented by blue beads) at a constant deformation velocity of 1×10^{-4} nm/ps. The high strain (up to 100%) employed in our CGMD simulations is to compensate the differences in the associated time and length scales (minutes in experiments compared to microseconds in CGMD simulations). Additionally, inherent rigidity of the CG force field due to low degrees of freedom is compensated by the high velocity of deformation [13].*

While constant velocity of deformation boundary condition is imposed along the longitudinal direction, constant pressure conditions (1 atm. pressure under Parrinello-Rahman barostat with 10^{-15} sec^{-1} as coupling constant) are applied along the transverse boundaries (*y*- and *z*-directions). GROMACS 2019.4 [38] is used for all the CGMD simulations and VMD 1.8.2 (Visual Molecular Dynamics) [39] for visualization of the molecular structures. The stress-strain distribution, as presented in Figure 2(a), is derived from moving average calculations (sampled every 20 ps) of

the p_{xx} component of the pressure tensor. Tensile (Young's) modulus is calculated from the slope of the linear region of stress-strain curve (Figure 2(a)). Glass transition temperature, T_g, is determined by fitting two straight lines to the two distinct linear regimes of the density profile during thermal quenching, which is performed by gradually decreasing the temperature of the simulation box, as shown in Figure 2(b).

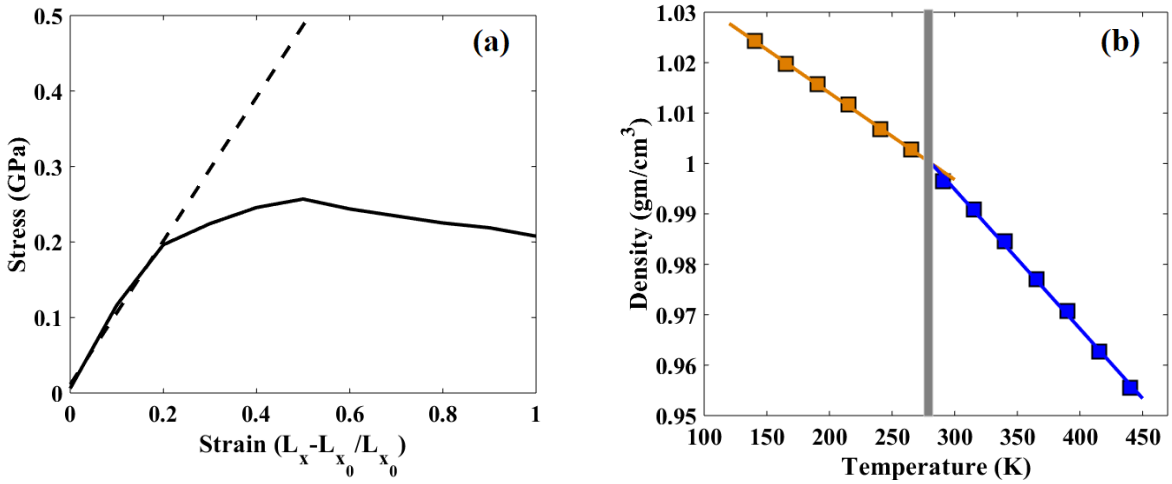

Figure 2: ***(a)*** *Stress as a function of strain (along the x-direction) during unidirectional straining of thermally annealed P3HT:PCBM BHJ. Tensile modulus (in GPa) is calculated from the slope of the linear part of the stress-strain curve.* ***(b)*** *Density as a function of temperature during thermal quenching of pure P3HT polymer. Glass transition temperature (T_g) is calculated from the change in the slope of the density profile. T_g = 281.44 K is found for 120-mer P3HT which is highlighted in gray.*

Morphological characterization: The computed morphology of P3HT:PCBM BHJ is discretized into small cubes of dimension ~ 0.5×0.5×0.5 nm^3 (a.k.a. voxels) consistent with the CG bead diameter of P3HT and PCBM inside the simulation box. Initially, the number of P3HT and PCBM beads inside each voxel are calculated and assigned with binary values (1 or 0) based on the type of beads inside the respective voxel. Figure S2 in the supplementary information presents the BHJ morphology for 1.0:0.8 weight ratio of P3HT:PCBM along with the corresponding discretization

sampled along *x*-*y* plane. Exciton diffusion, charge dissociation and charge transport in BHJ layers depend on three key morphological features, *viz.*, average domain size, interfacial area and percolation ratio [15]. These features are calculated from the volume occupied by each phase (P3HT or PCBM), total surface area of adjacent voxels containing P3HT and PCBM molecules, and the fraction of P3HT (or PCBM) voxels that create a continuous path to the surface (*i.e.*, the electrodes). Herman's orientation factors (f_i) [40, 41] for individual P3HT chains in pure P3HT and P3HT:PCBM BHJ morphology are calculated to characterize bond orientation of polymers in the bulk morphology by using 2nd order Legendre polynomials denoted as $f_i = \frac{3}{2}\left(\frac{1}{B_i}\sum_{j=1}^{B_i}\left(\cos\theta_j\right)^2\right) - \frac{1}{2}$, where $-\frac{1}{2} \leq f_i \leq 1$. In the equation [41], θ_j denotes the angle between the j^{th} backbone bond of the i^{th} polymer and the *x*-axis (for P3HT chain alignment in the longitudinal direction) and B_i denotes the total number of bonds in the backbone of the i^{th} P3HT chain. The orientation parameter (f) is finally computed by sampling f_i over all the P3HT molecules. The overall orientation factor f can take a value between -0.5 and 1.0 as mentioned above. When, $f \sim$ -0.5 all chains are aligned perpendicular to the axis in consideration (*x*-axis), $f \sim$ 1.0 all chains completely aligned with *x*-axis and $f \sim 0$ the system has no preferential orientation in any direction and hence indicates an isotropic nature of the phase.

Exciton diffusion to charge transport probability (P): Since charge dissociation occurs at the P3HT:PCBM interface, a correlation between exciton diffusion, charge dissociation and charge transport probability can provide insight into the morphology of the P3HT:PCBM BHJ. Inspired by the microscopic equation for IPCE (Incident photon to converted electron) ratio, developed in our earlier effort [42], we define exciton diffusion to charge transport probability (P) which correlates three dominant morphological features such as domain size, interfacial area to volume ratio and percolation ratio. Assuming all of the solar energy absorbed by both donor and acceptor

phases can generate excitons, the exciton diffusion to charge transport probability is denoted as, $P = P_{diff} * P_{diss} * P_{perc}$, where the probability of exciton diffusion $P_{diff} = \frac{1}{N_{box}} \sum_v e^{(-\frac{d}{\varepsilon_{exciton}})}$, probability of charge dissociation $P_{diss} = \frac{A_{int}}{V_{box}} * t_{int}$, probability of charge transport $P_{perc} = P_{P3HT} * P_{PCBM} * \frac{1}{N_{box}} \sum_v e^{\left(-\frac{S_A}{\varepsilon_h}\right)} * e^{\left(-\frac{S_C}{\varepsilon_e}\right)}$. These probabilities, in accordance with the morphological characterization discussed in the previous section, are calculated under the assumption of a finite element scheme by counting individual events (*viz.* exciton diffusion, dissociation and charge transport) for each small voxel (~ 0.5×0.5×0.5 nm^3) followed by the summation of all individual contributions as shown in the equations. A_{int} and t_{int} are interfacial area and interface thickness; V_{box} is volume of the simulation box and N_{box} is the number of voxels after discretizing the simulation box by finite element scheme [16, 37]. P_{P3HT} and P_{PCBM} are the corresponding percolation ratios of P3HT and PCBM phases, while d, S_A and S_C are respectively the shortest distances that an exciton needs to travel until it reaches an interface, a hole needs to travel to reach the anode, and that an electron needs to travel to reach the cathode. According to methods implemented in earlier effort [42], under the current discretization scheme each of these parameters are calculated for each voxel to calculate the probability for the 3D microstructure. Finally, $\varepsilon_{exciton}$, ε_h and ε_e are the properties of the donor and acceptor materials known as diffusion lengths of exciton, holes and electrons, respectively. Table 1 lists all the properties for P3HT:PCBM morphology considered in this work.

Table 1: *Material properties considered for the morphological characterization are listed for P3HT:PCBM BHJ system. Exciton diffusion, dissociation and charge transport are strongly dependent on the electronic properties such as exciton and charge diffusion through the photoactive layers.*

Parameters	Value	Reference

Exciton diffusion length ($\varepsilon_{exciton}$)	5.4 ± 0.7 nm	[43]
Electron diffusion length (ε_e)	340 nm	[44]
Hole diffusion length (ε_h)	90 nm	[44]

3. Results and Discussion

We perform CGMD simulations of solvent evaporation and thermal annealing of bulk morphology with pure P3HT molecules (chain lengths of 48-mer and 120-mer are considered). The density of 120-mer P3HT is calculated as ~ 0.99392 g/cm^3, which reasonably agrees with earlier experiments (~ 1.09 g/cm^3) [23].

Table 2: *Thermal and mechanical properties of pure P3HT polymers are presented. Results from CGMD simulations are validated against experimental results [45]. Close agreement between CGMD predictions and experiments corroborate our choice of potentials for the molecular modelling.*

	Glass transition (T_g) (K)		**Tensile modulus (GPa)**	
	CGMD	Experimental [45]	CGMD	Experimental [23]
Neat P3HT (48-mer)	280.50 ± 5.80	273.15	0.86 ± 0.19	
Neat P3HT (120-mer)	281.44 ± 15.60	285.1	1.33 ± 0.30	1.09 ± 0.15

Table 2 compares different thermomechanical properties predicted from CGMD simulations against corresponding experimental results [23, 45]. Glass transition temperature and tensile modulus, obtained from CGMD, concur with experiments, thereby validating our choice of force field used in the present work. From the mechanical response and corresponding calculation of Young's modulus, 120-mer P3HT can be inferred to have significantly large mechanical strength leading to a relatively stiffer material. Although failure due to chain pulling can be observed for 48-mer P3HT at strain > 200%, 120-mer P3HT does not demonstrate any onset of crack failure for

the range of strain rates considered in our simulations (Figures 3(a), (b)). It is important to note that experimentally crack onset occurs at a strain ~ 2% for P3HT:PCBM [46], and the absence of a crack in our simulations can be attributed to the nonexistence of interfacial impurity (*e.g.*, defects at the surface) that typically initiate cracks in the corresponding microstructures, as also discussed in earlier computational efforts [29]. We assume periodic boundary condition (PBC) in three directions which ignores any surface and interfacial effect including surface induced cracks affecting the mechanical response of the bulk morphology. Figure 3(c) presents the stress-strain behavior of P3HT for different degrees of polymerization, *i.e.*, 48-mer (blue) and 120-mer (red). Due to crack failure of 48-mer P3HT at strain > 200%, stress is reduced to ~ 0 GPa as observed in Figure 3(c). The variation in the orientation parameter as a function of the applied strain (Figure 3(d)) reveals an increased alignment of the polymer chains (48-mer P3HT) along the direction of strain, which eventually leads to the failure due to pulling of the chain at a high strain rate, as noted in Figure 3(a).

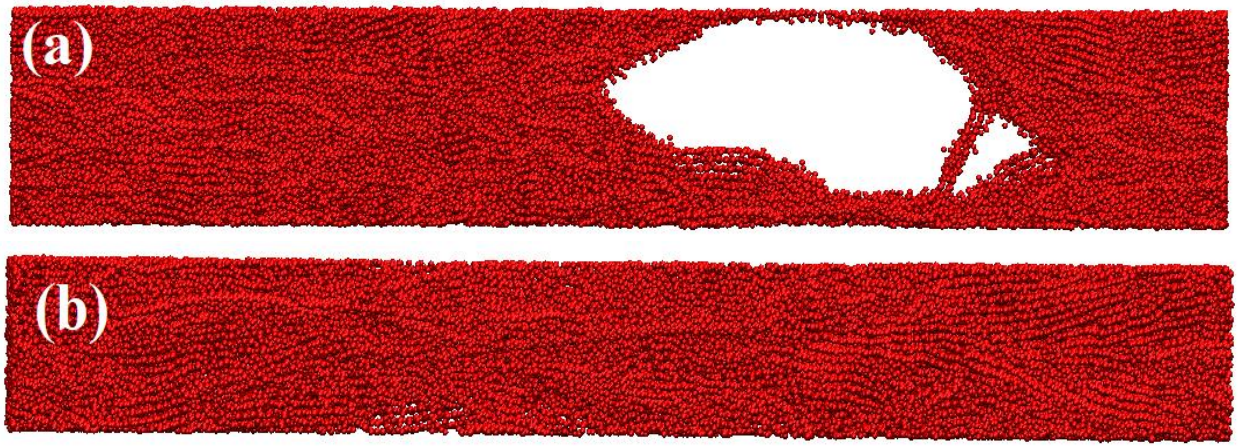

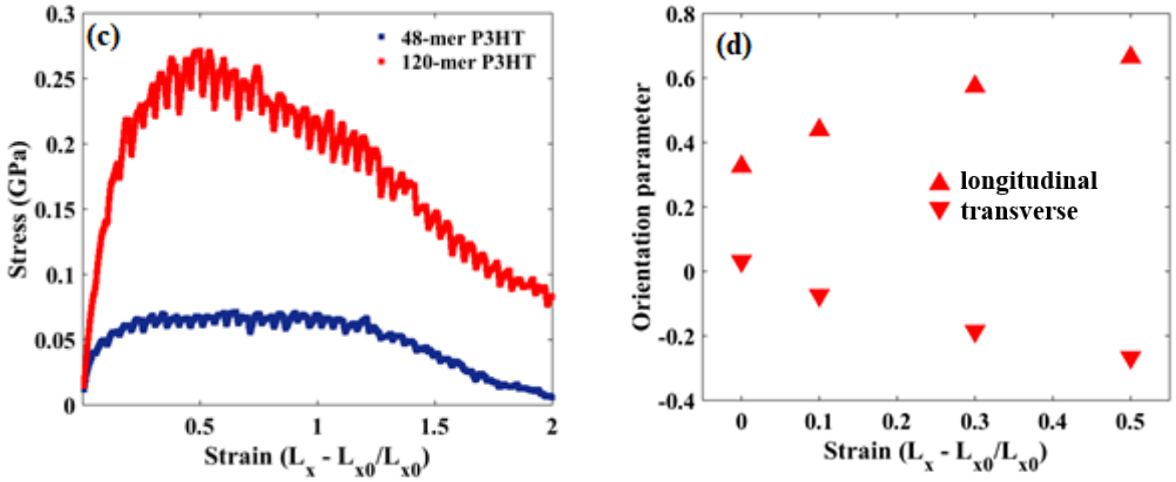

Figure 3: (a) *Visual inspection of P3HT polymer morphology for 48-mer reveals failure due to crack at 200% strain.* ***(b)*** *Visual inspection of 120-mer P3HT polymer morphology reveals no such phenomenon as observed for 48-mer P3HT for strain > 200%.* ***(c)*** *Stress-strain behavior for different P3HT chain lengths. The 48-mer P3HT shows reduction of stress to ~ 0 GPa at a strain ~ 200%. However nonzero stress is observed for strain rate > 200% for 120-mer P3HT* ***(d)*** *Orientation parameter in the x-direction (longitudinal) and y-direction (transverse) for 48-mer P3HT polymer is presented as a function of unidirectional strain. Gradual increase of longitudinal component of orientation parameter reveals alignment of polymers along the direction of applied strain.*

***Effect of PCBM weight fraction*:** We inspect the effect of PCBM as an acceptor material on the thermomechanical stability of P3HT:PCBM BHJ active layer. P3HT:PCBM based BHJs are one of the most studied and well understood systems for OSC device applications [47]. Solution processing parameters such as weight ratio of constituent materials, degree of polymerization, polydispersity of P3HT molecules and annealing temperature are known to affect the performance, morphology and thermomechanical stability of the BHJ layer. Research efforts in past decade revealed weight fraction of PCBM to be one of the most dominant design variables affecting the PCE of the OSC device [48-50]. Here, we investigate the effect of PCBM weight fraction on the mechanical properties of the BHJ active layers, and the results are reproduced in Figure 4. P3HT:PCBM BHJ active layers with different weight ratios of the constituent donor and acceptor

materials are simulated from a ternary mixture of P3HT:PCBM solvated in CB followed by thermal annealing of solvent-free P3HT:PCBM, as described in the Methods section as well as in the supplementary information. Glass transition temperature (T_g) of the mixture is calculated from the change in density as a function of temperature during the thermal quenching of the system (Figure 2(a)). Figure 4(a) reveals significant increase in T_g, in agreement with the previous experimental result [45], when PCBM is added as an acceptor material. T_g corresponds to the temperature at which the transition from amorphous glassy phase to a liquid like polymer-melt phase occurs. Knowledge of thermal properties related to glass transition is crucial for OSC applications as the aforementioned phase transition at a temperature ~ T_g is closely related to the choice of annealing temperature that determines the efficiency of OSC devices [18]. We find T_g for 1.0:1.0 weight ratio of P3HT:PCBM to be ~ 337 K. Glass transition for a range of PCBM weight fraction (~ 33 - 66% of PCBM mass loading) is predicted to be between 293 - 350 K. As thermal annealing is a post-evaporation step to achieve efficient BHJ microstructures by molecular rearrangements from a quasi-stable non-equilibrium morphology to a stable morphology, annealing temperature should be always maintained above glass transition temperature, T_g. We determine the tensile modulus and stress-strain behavior of thermally annealed P3HT:PCBM mixtures as shown in Figures 4(b) and (c), respectively. PCBM addition leads to a stiffer material with a larger tensile modulus indicating anti-plasticizing effect of PCBM. Figure 4(d) shows a trade-off between efficiency of BHJ layers quantified by exciton generation to charge transport probability (hereafter, referred to simply as ‘efficiency’) and tensile modulus of different P3HT:PCBM compositions. Higher efficiency is obtained for P3HT:PCBM with weight ratios ~ 1.0:0.8, in agreement with our recent effort on understanding the effect of solution processing parameters on BHJ morphology [18]. Figure 4(d) reveals that PCBM with a mass loading > 50%

can have adverse effect due to the inherent brittleness introduced by PCBM along with significant reduction in the efficiency. In light of the results presented in Figure 4(d), weight fraction of PCBM between 40 - 50% is concluded to be most promising due to a relatively high efficiency and flexibility of the P3HT:PCBM BHJ mixtures.

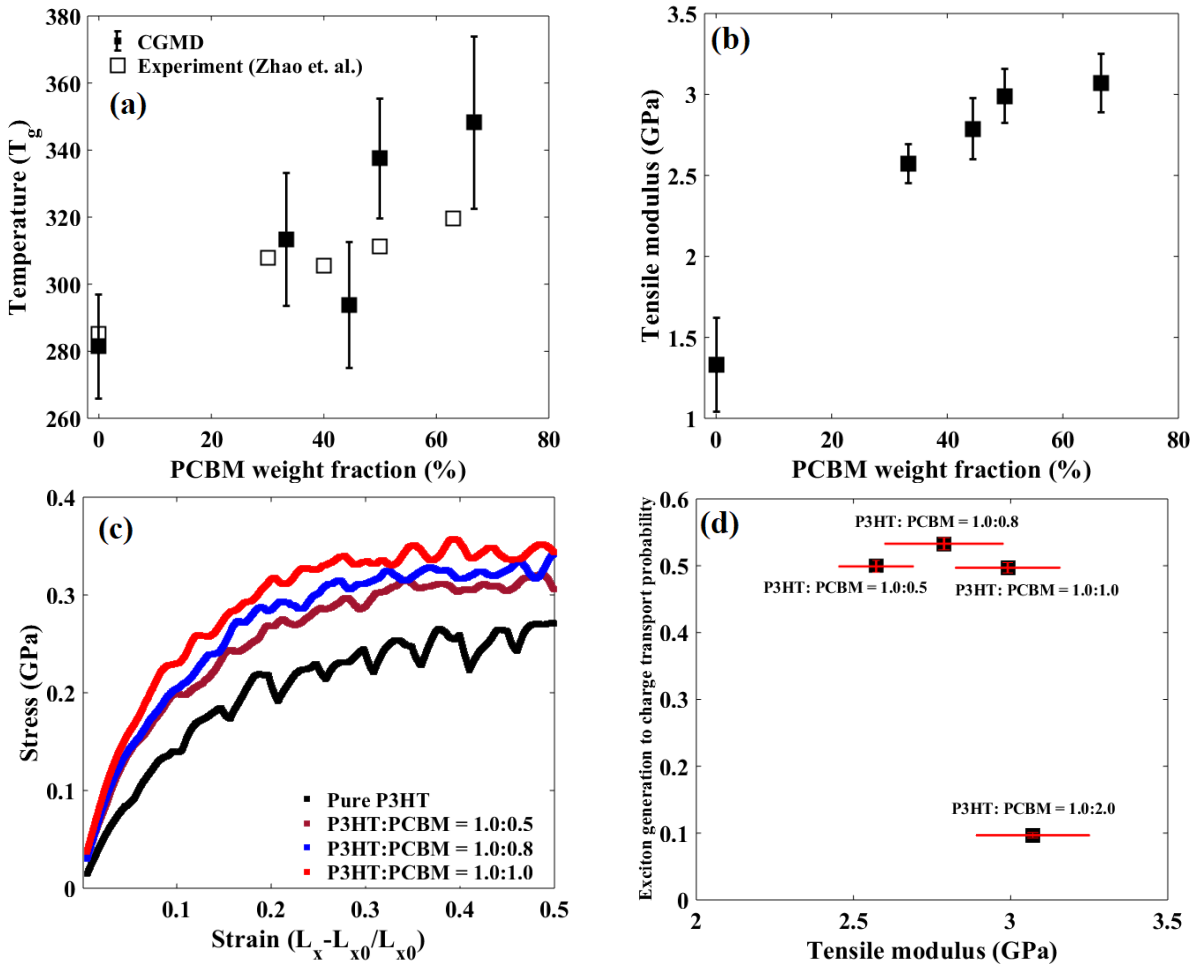

Figure 4: ***(a)*** *Glass transition temperature (T_g) as a function of PCBM weight fraction. The predicted trend of increasing T_g with increasing PCBM in the BHJ agrees with pervious experimental results [45].* ***(b)*** *Tensile modulus as a function of PCBM weight fraction. Addition of PCBM increases the tensile modulus of the BHJ layer indicating the anti-plasticizing effect of PCBM molecules.* ***(c)*** *Stress-strain response for different P3HT:PCBM weight ratios. Increase in the slope of the linear region of stress-strain curve reveals the BHJ becomes stiffer due to PCBM addition.* ***(d)*** *Exciton diffusion to charge transport probability as a function of tensile modulus for different P3HT:PCBM weight*

ratios. A 1.0:0.8 weight ratio is found to have the highest probability with relatively low tensile modulus indicating an optimum morphology for a flexible OSC active layer.

Effect of small molecule additive: Low molecular weight conjugated donor polymers (often known as oligomer), such as P3HT with chain length < 10, can significantly modify morphology of P3HT:PCBM BHJs affecting their mechanical as well charge transport properties. Carrillo *et. al.* [51] reported the beneficial effects of oligomeric additive insertions in improving the efficiencies of BHJ morphologies. The enhanced performance was attributed to the significant increase in the effective domain size and interfacial area due to the accumulation of small oligomer molecules at the interface between P3HT and PCBM. We simulate BHJs with P3HT oligomers (8-mer) as an additive to examine the thermomechanical response of the mixture. P3HT:PCBM:Oligomer ternary mixtures are prepared following the abovementioned two-step thin film synthesis following the solvent evaporation and thermal annealing protocols.

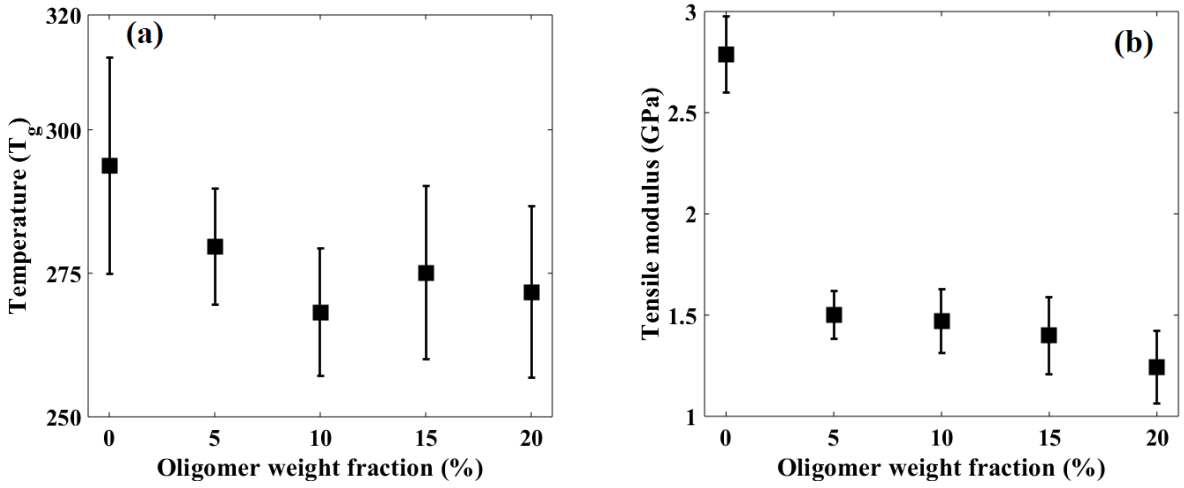

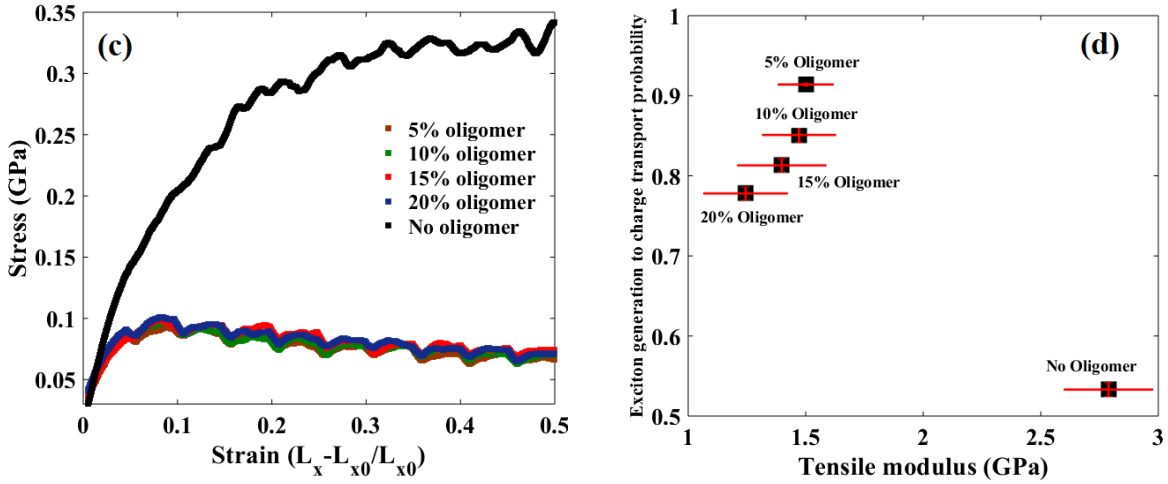

Figure 5: (a) *Glass transition temperature (T_g) as a function of weight percent oligomer additive (8-mer P3HT). T_g decreases to ~ 268 K for 20% oligomer additives indicating plasticizing effect of oligomers.* ***(b)*** *Tensile modulus for different oligomer additive content in 1.0:0.8 P3HT:PCBM BHJ. Decrease in tensile modulus can be attributed to the decrease in entanglement density due to small molecule inclusions.* ***(c)*** *Stress-strain response for different oligomer mass loading. Visual inspection reveals a decrease in the tensile modulus due to the presence of oligomer additives.* ***(d)*** *Exciton generation to charge transport probability as a function of the tensile modulus for various weight percentages of oligomers. Anti-plasticizing effect of PCBM reduces due to the oligomer inclusions as the tensile modulus reduces with increasing oligomer fraction. Addition of ~5% oligomers can be beneficial due to significant increase in efficiency in addition to the decrease in tensile modulus. However, the decrease in glass transition temperature below room temperature can lead to unstable morphology at operating temperatures > 300 K.*

Figure 5(a) presents the variations in T_g as a function of oligomer mass loading (weight fraction of oligomers in the ternary composite system). A gradual decrease in T_g (~ 268 K) with increase in oligomer mass loading implies the plasticizing effect of the oligomers in the BHJ. The plasticizing effect of oligomers contrasts partially the anti-plasticizing effect of PCBM molecules due to the low T_g of P3HT with chain lengths shorter than 10-mer [52]. The predicted reduction in T_g for P3HT:PCBM BHJ in presence of oligomer additives potentially contributes to an inherently unstable morphology for a broad range of operating temperatures, up to ~ 350 K. Despite the anticipated benefits of additive insertion, the morphological instability of the BHJ active layer in

presence of oligomer additives can lead to performance degradation. Additionally, tensile modulus is also predicted to decrease significantly due to the presence of oligomers, as shown in Figures 5(b) and (c). This behavior can be attributed to the higher miscibility of P3HT oligomers (due to their low molecular weight) in the composite system as opposed to the miscibility of longer chains of P3HT in PCBM, as also discussed in our earlier effort [17]. P3HT with chain length < 48 usually exhibits higher miscibility with PCBM for weight ratio of 1.0:0.8, facilitating the increase in an amorphous mixed phase consisting of P3HT and PCBM. The P3HT:PCBM:Oligomer system under investigation is considered to be equivalent to a polydisperse system of P3HT:PCBM with a bimodal distribution. Furthermore in our previous computational effort to investigate polydisperse P3HT:PCBM BHJ [37] we concluded increase in intermixing of small chains of P3HT molecules at the P3HT:PCBM interfaces. To explain the effect of enhanced miscibility, we compute the orientation parameters (both the longitudinal and transverse components) as a function of the oligomer mass loading, presented in Figure 6(a). The overall alignment of the P3HT phase significantly reduces ($f \sim 0$) upon addition of oligomers indicating enhanced intermixing and higher miscibility. The overall decrease in orientation (isotropic) due to oligomeric inclusion indicate loss of local molecular arrangements (semi-crystalline order) which is also responsible for loss of efficiency beyond a mass loading of oligomer (~ 5%). The trade-off between the computed efficiency and the tensile modulus of P3HT:PCBM BHJ as a function of oligomer mass loading is shown in Figure 5(d). An enhanced efficiency is obtained upon addition of oligomer molecules, especially when the mass loading is ~ 5%. The increase in efficiency with a corresponding increase in oligomer mass loading, also reported by Carrillo *et. al.* in their recent work [51], is also explained from the interfacial area to volume ratio (IAVR) (nm^{-1}), illustrated in Figure 6(b). The highest efficiency of a BHJ morphology with 5% mass loading of oligomers is attributed due to

the balance between miscibility (denoted by orientation) and the highest IAVR . Despite the enhanced flexibility due to reduction in the anti-plasticizing effect, the oligomeric insertion beyond 5% into the BHJ morphology demonstrates inefficient energy conversion capability (Figure 5(d)) along with an inherent thermo-mechanical instability (Figure 5(a)). Based on the findings presented in Figure 5, insertion of oligomers ≤ 5% is concluded to be beneficial due to significantly high efficiency and flexibility of the final morphology.

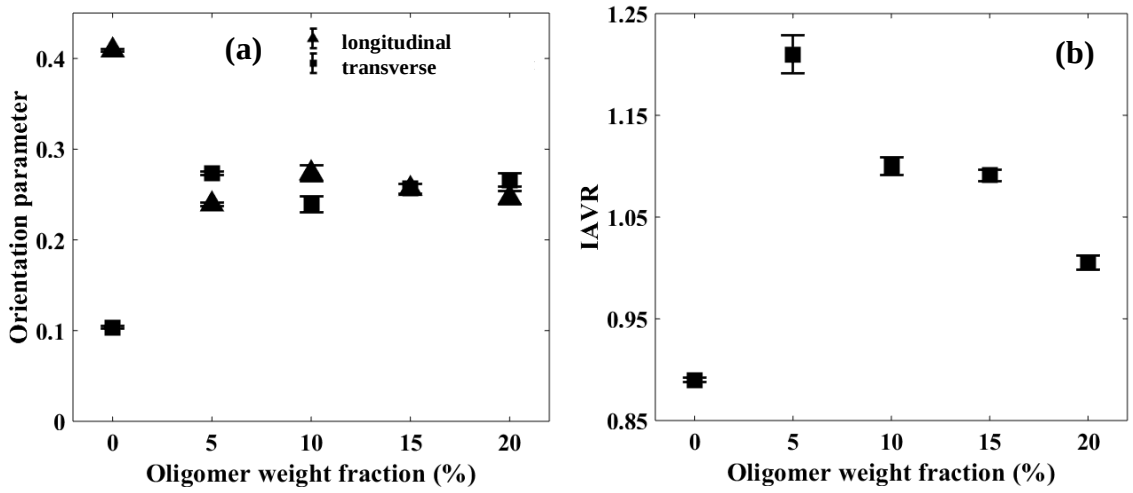

Figure 6: (a) *Orientation parameter in x-direction (longitudinal) and y-direction (transverse) for different weight fractions of oligomer additives in absence of unidirectional tensile strain. Effective orientation along longitudinal direction reduces due to oligomer insertion.* ***(b)*** *Interfacial area to volume ratio (IAVR) as a function of oligomer additive weight fraction (%). An increase in effective IAVR is responsible for the increase in efficiency (exciton generation to charge transport probability).*

4. Conclusion

In summary, CGMD simulations are employed to investigate the thermo- and elasto-mechanical properties of P3HT: PCBM BHJ systems typically used in OSC devices. Glass transition temperature and stress-strain behavior of pure P3HT polymers with different chain lengths are found to have excellent agreement with previous experimental reports. Introduction of PCBM

molecules as acceptor material is observed to increase both glass transition temperature and tensile modulus indicating anti-plasticizing effect of PCBM. This behavior is attributed to the significantly high glass transition temperature of pure PCBM leading to a stiffer material at room temperature upon annealing. BHJ mixture with ~ 1.0:0.8 P3HT:PCBM weight ratio is found to have the highest exciton generation to charge transport probability (efficiency) as well as relatively flexible morphology. Small chain length of P3HT, on the other hand, exhibits lower glass transition temperature and assumes lower values for the tensile modulus. Addition of small oligomer molecules in the BHJ hence partially limits the anti-plasticizing effect of PCBM. Despite the increase in efficiency of BHJ devices in presence of oligomer additives, morphological instability due to low glass transition temperature is anticipated to degrade the performance of OSCs over long periods of time at considerably higher operating temperatures above its glass transition.

Author Information

Corresponding Author

Ganesh Balasubramanian – Department of Mechanical Engineering and Mechanics, Lehigh University, Bethlehem, Pennsylvania 18015, USA; orcid.org/ 0000-0003-1834-5501; Email: bganesh@lehigh.edu.

Authors

Joydeep Munshi – Department of Mechanical Engineering and Mechanics, Lehigh University, Bethlehem, Pennsylvania 18015, USA.

TeYu Chien – Department of Physics and Astronomy, University of Wyoming, Laramie, Wyoming 82071, USA.

Wei Chen – Department of Mechanical Engineering, Northwestern University, Evanston, Illinois 60208, USA.

Author Contributions

JM performed all the simulations. JM and GB analyzed the computational results. The manuscript was written through contributions of all authors. All authors have given approval to the final version of manuscript.

Acknowledgments

This material is based on the work supported by the National Science Foundation (NSF) under Award Nos. CMMI-1662435, 1662509 and 1753770. JM and GB acknowledge the allocation of leadership class computing time on Frontera (at the Texas Advanced Computing Center (TACC) in The University of Texas at Austin) to perform the simulations. Any opinions, findings, conclusions or recommendations expressed in this material are those of the authors' and do not necessarily reflect the views of the NSF.

References

1. Kurtz, S., N. Haegel, R. Sinton, and R. Margolis, *A new era for solar.* Nature Photonics, 2017. **11**: p. 3.
2. Lai, C.S., Y. Jia, L.L. Lai, Z. Xu, M.D. McCulloch, and K.P. Wong, *A comprehensive review on large-scale photovoltaic system with applications of electrical energy storage.* Renewable and Sustainable Energy Reviews, 2017. **78**: p. 439-451.
3. Günes, S., H. Neugebauer, and N.S. Sariciftci, *Conjugated Polymer-Based Organic Solar Cells.* Chemical Reviews, 2007. **107**(4): p. 1324-1338.
4. Thompson, B.C. and J.M.J. Fréchet, *Polymer–Fullerene Composite Solar Cells.* Angewandte Chemie International Edition, 2008. **47**(1): p. 58-77.
5. Chen, L.-M., Z. Hong, G. Li, and Y. Yang, *Recent Progress in Polymer Solar Cells: Manipulation of Polymer:Fullerene Morphology and the Formation of Efficient Inverted Polymer Solar Cells.* Advanced Materials, 2009. **21**(14-15): p. 1434-1449.
6. Scharber, M.C. and N.S. Sariciftci, *Efficiency of bulk-heterojunction organic solar cells.* Progress in Polymer Science, 2013. **38**(12): p. 1929-1940.
7. Li, G., R. Zhu, and Y. Yang, *Polymer solar cells.* Nature Photonics, 2012. **6**: p. 153.
8. Lee, M.R., R.D. Eckert, K. Forberich, G. Dennler, C.J. Brabec, and R.A. Gaudiana, *Solar Power Wires Based on Organic Photovoltaic Materials.* Science, 2009. **324**(5924): p. 232-235.
9. Kaltenbrunner, M., M.S. White, E.D. Głowacki, T. Sekitani, T. Someya, N.S. Sariciftci, and S. Bauer, *Ultrathin and lightweight organic solar cells with high flexibility.* Nature Communications, 2012. **3**: p. 770.
10. Che, X., Y. Li, Y. Qu, and S.R. Forrest, *High fabrication yield organic tandem photovoltaics combining vacuum- and solution-processed subcells with 15% efficiency.* Nature Energy, 2018. **3**(5): p. 422-427.
11. Jackson, N.E., B.M. Savoie, T.J. Marks, L.X. Chen, and M.A. Ratner, *The Next Breakthrough for Organic Photovoltaics?* The Journal of Physical Chemistry Letters, 2015. **6**(1): p. 77-84.
12. Huang, Y., E.J. Kramer, A.J. Heeger, and G.C. Bazan, *Bulk Heterojunction Solar Cells: Morphology and Performance Relationships.* Chemical Reviews, 2014. **114**(14): p. 7006-7043.
13. Alessandri, R., J.J. Uusitalo, A.H. de Vries, R.W.A. Havenith, and S.J. Marrink, *Bulk Heterojunction Morphologies with Atomistic Resolution from Coarse-Grain Solvent Evaporation Simulations.* Journal of the American Chemical Society, 2017. **139**(10): p. 3697-3705.
14. Carrillo, J.-M.Y., R. Kumar, M. Goswami, B.G. Sumpter, and W.M. Brown, *New insights into the dynamics and morphology of P3HT:PCBM active layers in bulk heterojunctions.* Physical Chemistry Chemical Physics, 2013. **15**(41): p. 17873-17882.
15. Lee, C.-K., C.-W. Pao, and C.-W. Chu, *Multiscale molecular simulations of the nanoscale morphologies of P3HT:PCBM blends for bulk heterojunction organic photovoltaic cells.* Energy & Environmental Science, 2011. **4**(10): p. 4124-4132.
16. Ghumman, U.F., A. Iyer, R. Dulal, A. Wang, J. Munshi, T. Chien, G. Balasubramanian, and W. Chen, *A Spectral Density Function Approach for Design of Organic Photovoltaic Cells*, in *ASME IDETC/CIE Design Automation Conference*. 2018, ASME: Quebec City, Quebec, Canada.

17. Munshi, J., U. Farooq Ghumman, A. Iyer, R. Dulal, W. Chen, T. Chien, and G. Balasubramanian, *Composition and processing dependent miscibility of P3HT and PCBM in organic solar cells by coarse-grained molecular simulations.* Computational Materials Science, 2018. **155**: p. 112-115.
18. Munshi, J., R. Dulal, T. Chien, W. Chen, and G. Balasubramanian, *Solution Processing Dependent Bulk Heterojunction Nanomorphology of P3HT/PCBM Thin Films.* ACS applied materials & interfaces, 2019. **11**(18): p. 17056-17067.
19. Yang, C.Y. and A.J. Heeger, *Morphology of composites of semiconducting polymers mixed with C60.* Synthetic Metals, 1996. **83**(2): p. 85-88.
20. Stingelin-Stutzmann, N., E. Smits, H. Wondergem, C. Tanase, P. Blom, P. Smith, and D. de Leeuw, *Organic thin-film electronics from vitreous solution-processed rubrene hypereutectics.* Nature Materials, 2005. **4**: p. 601.
21. Jørgensen, M., K. Norrman, and F.C. Krebs, *Stability/degradation of polymer solar cells.* Solar Energy Materials and Solar Cells, 2008. **92**(7): p. 686-714.
22. Kleinschmidt, A.T., S.E. Root, and D.J. Lipomi, *Poly(3-hexylthiophene) (P3HT): fruit fly or outlier in organic solar cell research?* Journal of Materials Chemistry A, 2017. **5**(23): p. 11396-11400.
23. Savagatrup, S., A.S. Makaram, D.J. Burke, and D.J. Lipomi, *Mechanical Properties of Conjugated Polymers and Polymer-Fullerene Composites as a Function of Molecular Structure.* Advanced Functional Materials, 2014. **24**(8): p. 1169-1181.
24. Savagatrup, S., A.D. Printz, D. Rodriquez, and D.J. Lipomi, *Best of Both Worlds: Conjugated Polymers Exhibiting Good Photovoltaic Behavior and High Tensile Elasticity.* Macromolecules, 2014. **47**(6): p. 1981-1992.
25. Müller, C., *On the Glass Transition of Polymer Semiconductors and Its Impact on Polymer Solar Cell Stability.* Chemistry of Materials, 2015. **27**(8): p. 2740-2754.
26. Roth, B., S. Savagatrup, N. V. de los Santos, O. Hagemann, J.E. Carlé, M. Helgesen, F. Livi, E. Bundgaard, R.R. Søndergaard, F.C. Krebs, and D.J. Lipomi, *Mechanical Properties of a Library of Low-Band-Gap Polymers.* Chemistry of Materials, 2016. **28**(7): p. 2363-2373.
27. Kim, J.-S., J.-H. Kim, W. Lee, H. Yu, H.J. Kim, I. Song, M. Shin, J.H. Oh, U. Jeong, T.-S. Kim, and B.J. Kim, *Tuning Mechanical and Optoelectrical Properties of Poly(3-hexylthiophene) through Systematic Regioregularity Control.* Macromolecules, 2015. **48**(13): p. 4339-4346.
28. Dulal, R., A. Iyer, U.F. Ghumman, J. Munshi, A. Wang, G. Balasubramanian, W. Chen, and T. Chien, *Elongated Nanodomains and Molecular Intermixing Induced Doping in Organic Photovoltaic Active Layers with Electric Field Treatment.* ACS Applied Polymer Materials, 2020. **2**(2): p. 335-341.
29. Root, S.E., S. Savagatrup, C.J. Pais, G. Arya, and D.J. Lipomi, *Predicting the Mechanical Properties of Organic Semiconductors Using Coarse-Grained Molecular Dynamics Simulations.* Macromolecules, 2016. **49**(7): p. 2886-2894.
30. Root, S.E., N.E. Jackson, S. Savagatrup, G. Arya, and D.J. Lipomi, *Modelling the morphology and thermomechanical behaviour of low-bandgap conjugated polymers and bulk heterojunction films.* Energy & Environmental Science, 2017. **10**(2): p. 558-569.
31. Tummala, N.R., C. Bruner, C. Risko, J.-L. Brédas, and R.H. Dauskardt, *Molecular-Scale Understanding of Cohesion and Fracture in P3HT:Fullerene Blends.* ACS Applied Materials & Interfaces, 2015. **7**(18): p. 9957-9964.

32. Munshi, J. and G. Balasubramanian, *Investigating blend morphology of P3HT:PCBM bulk heterojunction solar cells by classical atomistic simulations – Progress and prospects.* Soft Materials, 2020: p. 1-14.
33. Marrink, S.J. and D.P. Tieleman, *Perspective on the Martini model.* Chemical Society Reviews, 2013. **42**(16): p. 6801-6822.
34. Monticelli, L., *On Atomistic and Coarse-Grained Models for C60 Fullerene.* Journal of Chemical Theory and Computation, 2012. **8**(4): p. 1370-1378.
35. Panizon, E., D. Bochicchio, L. Monticelli, and G. Rossi, *MARTINI Coarse-Grained Models of Polyethylene and Polypropylene.* The Journal of Physical Chemistry B, 2015. **119**(25): p. 8209-8216.
36. Vögele, M., C. Holm, and J. Smiatek, *Coarse-grained simulations of polyelectrolyte complexes: MARTINI models for poly(styrene sulfonate) and poly(diallyldimethylammonium).* The Journal of Chemical Physics, 2015. **143**(24): p. 243151.
37. Munshi, J., U.F. Ghumman, A. Iyer, R. Dulal, W. Chen, T. Chien, and G. Balasubramanian, *Effect of polydispersity on the bulk-heterojunction morphology of P3HT:PCBM solar cells.* Journal of Polymer Science Part B: Polymer Physics, 2019. **57**(14): p. 895-903.
38. Abraham, M.J., T. Murtola, R. Schulz, S. Páll, J.C. Smith, B. Hess, and E. Lindahl, *GROMACS: High performance molecular simulations through multi-level parallelism from laptops to supercomputers.* SoftwareX, 2015. **1-2**: p. 19-25.
39. Humphrey, W., Dalke, A., Schulten, K., *VMD - Visual Molecular Dynamics*. J. Molec. Graphics, 1996. **14**: p. 33-38.
40. White, J.L. and J.E. Spruiell, *The specification of orientation and its development in polymer processing.* Polymer Engineering & Science, 1983. **23**(5): p. 247-256.
41. Pal, S., G. Balasubramanian, and I.K. Puri, *Modifying thermal transport in electrically conducting polymers: Effects of stretching and combining polymer chains.* The Journal of chemical physics, 2012. **136**(4): p. 044901.
42. Farooq Ghumman, U., A. Iyer, R. Dulal, J. Munshi, A. Wang, T. Chien, G. Balasubramanian, and W. Chen, *A Spectral Density Function Approach for Active Layer Design of Organic Photovoltaic Cells.* Journal of Mechanical Design, 2018. **140**(11).
43. Mikhnenko, O.V., H. Azimi, M. Scharber, M. Morana, P.W. Blom, and M.A. Loi, *Exciton diffusion length in narrow bandgap polymers.* Energy & Environmental Science, 2012. **5**(5): p. 6960-6965.
44. Tumbleston, J.R., D.-H. Ko, E.T. Samulski, and R. Lopez, *Nonideal parasitic resistance effects in bulk heterojunction organic solar cells.* Journal of Applied Physics, 2010. **108**(8): p. 084514.
45. Zhao, J., A. Swinnen, G. Van Assche, J. Manca, D. Vanderzande, and B.V. Mele, *Phase Diagram of P3HT/PCBM Blends and Its Implication for the Stability of Morphology.* The Journal of Physical Chemistry B, 2009. **113**(6): p. 1587-1591.
46. Savagatrup, S., A.D. Printz, T.F. O'Connor, A.V. Zaretski, D. Rodriquez, E.J. Sawyer, K.M. Rajan, R.I. Acosta, S.E. Root, and D.J. Lipomi, *Mechanical degradation and stability of organic solar cells: molecular and microstructural determinants.* Energy & Environmental Science, 2015. **8**(1): p. 55-80.
47. Dang Minh, T., L. Hirsch, and G. Wantz, *P3HT:PCBM, Best Seller in Polymer Photovoltaic Research.* Advanced Materials, 2011. **23**(31): p. 3597-3602.

48. Chirvase, D., J. Parisi, J.C. Hummelen, and V. Dyakonov, *Influence of nanomorphology on the photovoltaic action of polymer–fullerene composites.* Nanotechnology, 2004. **15**(9): p. 1317.
49. Hoppe, H., M. Niggemann, C. Winder, J. Kraut, R. Hiesgen, A. Hinsch, D. Meissner, and N.S. Sariciftci, *Nanoscale Morphology of Conjugated Polymer/Fullerene-Based Bulk-Heterojunction Solar Cells.* Advanced Functional Materials, 2004. **14**(10): p. 1005-1011.
50. Yang, X., J. Loos, S.C. Veenstra, W.J.H. Verhees, M.M. Wienk, J.M. Kroon, M.A.J. Michels, and R.A.J. Janssen, *Nanoscale Morphology of High-Performance Polymer Solar Cells.* Nano Letters, 2005. **5**(4): p. 579-583.
51. Carrillo, J.-M.Y., Z. Seibers, R. Kumar, M.A. Matheson, J.F. Ankner, M. Goswami, K. Bhaskaran-Nair, W.A. Shelton, B.G. Sumpter, and S.M. Kilbey, *Petascale Simulations of the Morphology and the Molecular Interface of Bulk Heterojunctions.* ACS Nano, 2016. **10**(7): p. 7008-7022.
52. Xie, R., Y. Lee, M.P. Aplan, N.J. Caggiano, C. Müller, R.H. Colby, and E.D. Gomez, *Glass Transition Temperature of Conjugated Polymers by Oscillatory Shear Rheometry.* Macromolecules, 2017. **50**(13): p. 5146-5154.

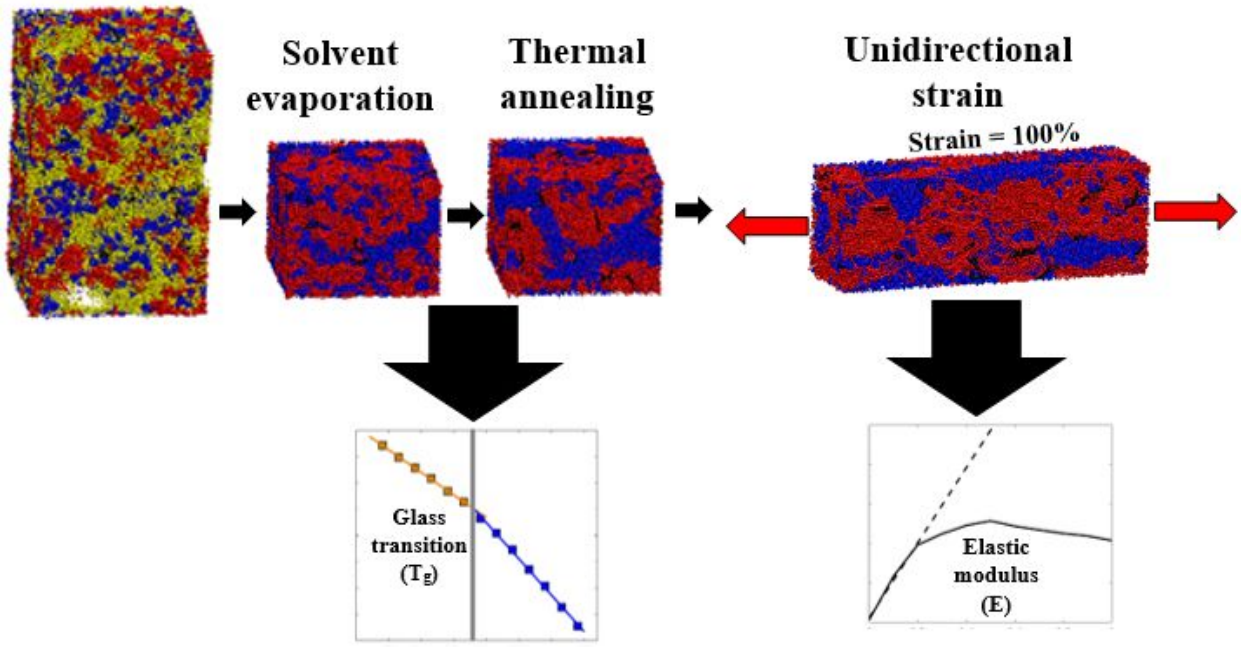

Effect of solution processing conditions on the elasto-morphology of bulk heterojunction layer reveal a trade-off between thermo-mechanical stability and performance in organic solar cells